NASA Technical Memorandum 108807

Backward-Facing Step Measurements at Low Reynolds Number, Re_h=5000

Srba Jovic, Eloret Institute, Palo Alto, California
David M. Driver, Ames Research Center, Moffett Field, California

February 1994

National Aeronautics and
Space Administration

Ames Research Center
Moffett Field, California 94035-1000

Backward-Facing Step Measurements at Low Reynolds Number, Re_h=5000

Srba Jovic* and David M. Driver
Ames Research Center

Summary

An experimental study of the flow over a backward-facing step at low Reynolds number was performed for the purpose of validating a direct numerical simulation (DNS) which was performed by the Stanford/NASA Center for Turbulence Research. Previous experimental data on backstep flows were conducted at Reynolds numbers and/or expansion ratios which were significantly different from that of the DNS. Consequently, the comparisons with existing data were poor, thus casting doubt on the DNS results.

The geometry of the experiment and the simulation were duplicated precisely, in an effort to perform a rigorous validation of the DNS. The Reynolds number used in the DNS was Re_h = 5100 based on step height, h. This was the maximum possible Reynolds number that could be economically simulated. The boundary layer thickness, δ,was approximately 1.0h in the simulation and the expansion ratio was 1.2. The Reynolds number based on the momentum thickness, Re_θ, upstream of the step was 610. All of these parameters were matched experimentally.

Experimental results are presented in the form of tables, graphs and a floppy disk (for easy access to the data). An LDV instrument was used to measure mean velocity components and three Reynolds stresses components ($\overline{uu}$, $\overline{vv}$, and $-\overline{uv}$). In addition, surface pressure and skin friction coefficients were measured. LDV measurements were acquired in a measuring domain which included the recirculating flow region.

*Eloret Institute

Nomenclature

C_{f0}	skin friction coefficient, $2\,\tau_w/\rho U^2_o$
C_f	local skin friction coefficient, $2\,\tau_w/\rho U^2_e$
C_p	pressure coefficient, $2(p-p_0)/\rho U^2_o$
G	Clauser parameter, $G = \frac{(H-1)}{H\sqrt{C_f/2}}$
h	step height
H	shape factor
p	wall static pressure
p_0	reference wall static pressure
Re_h	step height Reynolds number, U_0 h/ν
Re_θ	momentum thickness Reynolds number, $U_0\,\theta/\nu$
U_0	upstream freestream reference velocity
U	mean velocity in streamwise direction
u_τ	friction velocity
u, v	fluctuating velocity components in x and y directions respectively
$\overline{uu}$, $\overline{vv}$	normal Reynolds stresses

$-\overline{uv}$	Reynolds shear stress
x_r	mean reattachment length
x, y	coordinate system representing streamwise and wall-perpendicular directions measured from the step and the wall respectively
y^+	normalized distance from the wall, yu_τ/ν
ν	molecular kinematic viscosity of air, nominally $1.5*10^{-5} m^2/s$ at T = 20°C
ρ	air density, 1.2 kg/m^3 at T = 20°C
δ	boundary layer thickness where $U = 0.99U_e$
δ^*	displacement thickness
θ	momentum thickness
τ_w	wall shear stress

Introduction

The present experimental effort was motivated by a cooperative project on complex flows between the Modeling and Experimental Validation Branch of NASA Ames and the Stanford/NASA Ames Center for Turbulence Research. A Direct Numerical Simulation (DNS) of a backward-facing step configuration was chosen as the simplest geometry to generate a flow with separation that is equally suitable for experiments and computations (Le, Moin and Kim (1993a,b)). Reynolds number of the DNS is limited by the available computer memory and speed to resolve all time and length scales of turbulence. Thus, the DNS predictions were confined to a low step height Reynolds number, Re_h, of nominally 5000, for which there were no experimental data to compare. Consequently, an experiment was devised to match the conditions of the DNS. The experiment was carried out in a wind tunnel with a double-sided symmetrical sudden expansion to simulate the DNS single-sided expansion with a slip condition on the upper boundary of the computational domain.

The flow field of a separated flow is divided into four zones which are mutually interrelated. The zones are: the separated shear layer, the recirculating region under the shear layer, the reattachment region, and the attached/recovery region. Each flow region beares some resemblance to flows such as mixing layers and boundary layers. For the most part, the internal shear layer, which develops within the original boundary layer downstream of the step, appears to be similar to that of a plane mixing layer.

The objective of the present report is to present measurements of mean velocity, U, and Reynolds stress components, $\overline{uu}$, $\overline{vv}$, and - $\overline{uv}$ of the flow behind a backward-facing step for the purpose of rigorously validating the recent DNS computations of the same flow.

Wind Tunnel and Experimental Techniques

The experiment was conducted in a suction-driven open-return wind tunnel in the Modeling and Experimental Validation Branch of NASA Ames Research Center. The wind tunnel is shown schematically in Figure 1. Flow enters through a settling chamber containing a honeycomb and a set of three fine screens used for the flow conditioning. Flow continues through the two-dimensional 6:1 contraction before entering the developing section. The boundary layer develops on the walls of a 9.6 cm high by 30.5 cm wide by 46 cm long zero-pressure-gradient duct before passing into a sudden double-sided expansion. The tunnel expands symmetrically at the location of the step. The step height, h, on each side of the tunnel was nomi-

nally 0.98 cm which results in expansion ratio, E_r, of 1.2. The tunnel side walls were slightly diverged to compensate for the blockage effect due to boundary layer growth. The wall divergence was set to create a zero-pressure-gradient in both the upstream portion of the tunnel where the boundary layer develops as well as the region downstream of reattachment. Measurements were made at a reference flow speed, U_0, of 7.72 m/s measured at a station 3.0 cm upstream of the step. A free stream turbulence intensity was less than 1%.

A boundary layer trip wire (1.6 mm dia), was placed on all four walls of the wind tunnel (at 7.6 cm downstream of the entrance to the test-section) to ensure that the boundary layer was transitioned to turbulence uniformly along the span. The resulting boundary layer thickness was 1.15 cm (or 1.2h) at x=-3.05h upstream of the step. This was sufficiently close to the value of 1.0h obtained in the simulation. The Reynolds number, Re_θ, based on the momentum thickness was nominally 610 in both the simulation and the experiment. The integral parameters for the boundary layer at this location indicate that the boundary layer closely resembles that of a standard, fully developed zero-pressure-gradient turbulent boundary layer.

Table 1. Integral parameters and skin friction coefficient at x/h = -3.05

δ(cm)	δ^*(cm)	θ(cm)	H	10^3*C_f
1.15	0.17	0.12	1.45	4.9

Table 2. Maximum values of characteristic turbulent quantities at x/h=-3.05

u_{rms}/u_τ	v_{rms}/u_τ	$-\overline{uv}/u_\tau^2$	R_{uv}
2.90	0.82	0.811	0.51

Values of the integral parameters are shown in Table 1. The maximum values of $\overline{uu}$, $\overline{vv}$, $-\overline{uv}$, and R_{uv} for the upstream location are shown in Table 2. The characteristic maximum values of the measured Reynolds stresses indicate that the boundary layer is slightly overstimulated by the tripping device (Erm and Joubert (1991)). No attempt was made to correct this. The aspect ratio (tunnel width/ step height) of 31 is much greater than the value of 10 recommended by de Brederode snd Bradshaw (1972) as the minimum to assure two-dimensionality of a separated flow.

Instrumentation

Surface static pressures were measured on the upper and the lower (step-side) walls using a 10 Torr (1300 N/m^2) Barocel Transducer.

Mean and fluctuating velocities were measured with a dual-beam, two-component, fiber-optic laser Doppler velocimeter (LDV), which uses blue and green light (λ = 488 nm and 514.5 nm) from an argon ion laser for the vertical and streamwise components of velocity, respectively (see fig. 2). The fringes formed at the intersection of the blue beam pair (vertical component) were spaced 7.37 μm apart and the green fringes were spaced 35 μm. Each velocity component had one of its two beams bragg shifted by 40 MHz so as to create a bias in the frequency of the measured signal, thus allowing the instrument to distinguish the direction that the particle is traveling as well as the speed. Each of the four beams were intersected at a point inside the wind tunnel (known as the scattering volume) which measured 0.15 mm in diameter and 1 mm in length. Tiny (1 μm) water droplets (suspended in the air flow) scattered laser light as they passed through the scattering volume. The scattered light was collected by a lens which focused the light into a fiber through which it traveled to a dichroic light filter that spatially separated the green laser light from the blue before passing into their respective photomultiplier tubes. The electrical signals

were then filtered and processed in each of two TSI counters (model 1990). Only those signals that arrived simultaneously ($\pm$ 10 μs) were accepted and recorded by the computer. Those validated velocity pairs were ensemble averaged to obtain statistical measure of U, V, $\overline{uu}$, $\overline{vv}$, and $-\overline{uv}$. After considering the systematic and random errors as well as repeatability of measurements it was estimated that mean velocities were measured with $\pm$ 2% accuracy and the Reynolds stresses were measured with ±15% accuracy.

An Oil-Flow Laser Interferometer is used to make direct measurements of skin friction (see fig. 3). In this technique, a patch of oil which is placed on the wind tunnel floor will flow due to surface shear and a laser interferometer is used to measure the thickness of this patch of oil as a function of time. The interferometer senses the incident laser light which is reflecting from the air-oil interface as well as from the metal surface (light reflecting from the surface passes through the oil) as shown in figure 4. The two reflecting beams are received at a photodiode where either constructive or distractive interference takes place depending on the path length of the light which passes through the oil. The sinusoidal-like signal produced by the photodiode is used to determine the change in thickness of the oil as a function of time, from which the magnitude of the surface shear (acting on the oil) was determined using hydraulic theory. Skin friction was measured on the step-side wall with an uncertainty in the skin friction coefficient of less than ±0.0005 (based on an estimate of the systematic errors as well as repeatability). More detailed description of the method can be found in Monson, Driver and Szodruch (1981) and Monson and Higuchi (1981).

Results

Surface Pressure Distributions

The wall static-pressure coefficient is defined as

$$C_p = \frac{2(p - p_o)}{\rho U_o^2}$$

where p is the wall static pressure at any x location and p_o is the reference wall static pressure measured at x_o/h=-5.1 upstream of the step. The pressure-coefficient distribution measured in the plane of symmetry along the bottom and top walls are shown in figure 5. Most of the pressure recovery occurs within 10h of the step. Symmetry of the pressure distribution along the two walls demonstrates that the flow was symmetrical with approximately equal reattachment lengths on top and bottom walls.

Pressure-coefficient measurements are presented in tables 3 and 4.

Skin Friction Distributions

The skin-friction coefficient, C_f, shown in figure 6, is defined as

$$C_{f0} = \frac{2\tau_w}{\rho U_o^2}$$

where $\rho U_o^2/2$ is the reference dynamic head upstream of the step. Scatter of the data shows the error band of the experimental technique. Local skin-friction coefficients were used for normalization of the mean velocity and measured Reynolds stresses on wall variables in the recovery region of the flow. The large minimum value of the skin-friction coefficient of about -0.003 occurs about $0.67X_r$ downstream of the step in the recirculating region. This value is about three times larger than the minimum C_f measured for high Reynolds number of Driver and Seegmiller (1985), Westphal et al. (1984), and Adams et al.

(1984). Jovic and Driver (to be published) experimentally examined the relationship between minimum C_f and Re_h and found that the minimum skin friction-coefficient is a strong function of Re_h, increasing sharply for lower Reynolds numbers.

The reattachment length is deduced in two independent ways and was found to be $X_r/h = 6\pm0.15$. The mean reattachment length was determined from the oil flow visualization using a low viscosity oil. A second approach involving an interpolation of the measured skin-friction coefficient to find the point where $C_f = 0$. The reattachment length obtained by DNS is 6.0h based on the zero-crossing of their C_f distribution.

Mean velocity

Flow field velocities and Reynolds stresses of the evolving turbulent separated flow were measured at six streamwise locations. Mean velocity is shown in figure 7 in global coordinates (U/U_o vs. y/h) and in Figure 8 in wall coordinates. The first location at x/h = -3.05 was chosen to establish the state of the incoming low-Reynolds number turbulent boundary layer. The Reynolds number based on the momentum thickness at this location was Re = 610. The location, x/h = 4.0, is approximately the location where the minimum C_f and the maximum Reynolds stresses occur. The x/h = 6.0 location is where flow attaches in a time-average sense, while stations, x/h = 10, 15 and 19, were in the recovery region of the flow.

Mean velocity scaled with inner-wall variables (fig. 8) suggests that the reattached boundary layer is far from equilibrium. Deviations of the mean velocity from the law-of-the-wall were observed by Driver (1991) for a turbulent boundary layer prior to separation due to an adverse pressure gradient and by Jovic (to be published as NASA TM) for a recovering boundary layer downstream of a backward-facing step for different Reynolds numbers. The flow at reattachment and for some distance downstream resembles that of the mixing layer (emanating from the lip of the step) and does not develop with much near-wall similarity over this region. It appears that the remnants of the turbulent mixing layer dominate the entire boundary layer in the vicinity of reattachment and for some distance downstream. The wall appears to influence only a thin viscous region very near to the wall. Chandrsuda and Bradshaw (1981) and Jovic (1993), analyzing the balance of turbulent kinetic energy, showed that the recovering flow downstream of the mean reattachment point is far from equilibrium (production of turbulent kinetic energy is not equal to the rate of dissipation).

Measured mean velocity and the Reynolds stress data are listed in tables 5 through 10 of the Appendix.

Reynolds stresses

Profiles of Reynolds-stresses, $\overline{uu}$, $\overline{vv}$, and $-\overline{uv}$ normalized by U^2_o are shown in Figures 9, 10 and 11 respectively. All turbulent Reynolds stresses increase rapidly from the point of separation until about $0.67X_r$ where they reach a maximum. This rapid growth resembles that of the near field of a free shear layer. Beyond this point turbulence activity decays and gradually approaches the stress levels seen in an equilibrium boundary layer.

In the recovery region, Reynolds stresses normalized with wall coordinates, using the local C_f are shown in figures 12 through 14. The Reynolds stresses in the inner layer recover to levels comparable to that of an ordinary turbulent boundary layer (simulated by Spalart (1988)) by the time the flow reaches the x/h = 19 station. However, in the outer layer the Reynolds stresses decay much more slowly, owing to the persistence of large eddies which were gener-

ated in the shear layer upstream. These stresses in the outer region persist at high levels until quite far downstream (probably 100h), unlike the stresses in the inner region of the flow which converge to an equilibrium level within 25h to 30h of the step according to Jovic (1993).

Concluding remarks

A joint effort between the Modeling and Experimental Validation Branch of NASA Ames and Stanford/NASA Ames Center for Turbulence Research was conducted to understand the flow physics of the separating and reattaching turbulent boundary layer behind a backward-facing step.

Backward facing step flows are sensitive to step height Reynolds number, Re_h, (Jovic, to be published as a NASA TM), expansion ratio, and δ/h making it necessary to perform another backward-facing step flow experiment which closely duplicated the DNS conditions.

In the recovery region of the flow, the log-law of the mean velocity is not obeyed and does not exist as has been seen in previous sets of data (Driver-Seegmiller). This was also seen in Jovic (to be published as a NASA TM) for a number of different Reynolds numbers and levels of perturbation.

The results of this experiment show that the flow structure at this low Reynolds number is qualitatively similar to structures of flows at much higher Reynolds numbers. However, the magnitudes of turbulent quantities are dependent primarily on the Reynolds number, Re_h, and the strength of perturbation expressed by δ/h.

References

1. Adams, E.W., Johnston, J.P. and Eaton, J.K.: Experiments on the structure of turbulent reattaching flow. Report MD-43, Department of Mechanical Engineering, Stanford University, 1984.

2. Chandrsuda, C. and Bradshaw, P.: Turbulence structure of a reattaching mixing layer. J. Fluid Mech. 110, 1981, pp.171-194.

3. Driver, D.M. and Seegmiller, H.L.: Features of a reattaching turbulent shear layer in divergent channel flow, AIAA J. 23, 1985 , p.163.

4. Driver, D.M.: Reynolds shear stress measurements in a separated boundary layer flow. AIAA Paper 91-1787, Honolulu Hawaii Meeting, 24-27 June, 1991.

5. deBredorod, V. and Bradshaw, P.: Three-dimensional flow in nominally two-dimensional separation bubbles. Flow behind a rearward-facing step. I.C. Aero Report 72-19.13, 1972.

6. Erm,L.P. and Joubert, P.N.: Low-Reynolds number turbulent boundary layer. J. Fluid Mech., **230**, 1991, pp.1-44.

7. Jovic, S.: An experimental study on the recovery of a turbulent boundary layer downstream of the reattachment. Proceedings of the Second International Symposium on Engineering Turbulence Modelling and Measurements, Florence, Italy, 31 May-2 June, 1993.

8. Le, H., Moin, P. and Kim, J.: Direct numerical simulation of turbulent flow over a backward-facing step. Report TF-58, Thermosciences Division, Department of Mechanical Engineering, Stanford University, 1993.

9. Le, H., Moin, P. and Kim, J.: Direct numerical simulation of turbulent flow over a backward-facing step. 9th Symposium on Turbulent Shear Flows, Tokyo, 1993.

10. Monson, D., Driver, M.D. and Szodruch, J.: Applica-

tion of a Laser Interferometer skin-friction meter in complex flows. ICIASF'81 Record, International congress on Instrumentation in Aerospace Simulation Facilities, 1981, pp.232-243.

11. Monson, d. and Haguchi, H.: Skin Friction measurements by a dual-laser-beam interferometer technique, AIAA J. 19, 1981, p.739.

12. Spalart, P.R.: Direct simulation of a turbulent boundary layer up to Re=1410. J. Fluid Mech. 187, 1988, pp.61-98.

13. Westphal, R.V., Johnston, J.P. and Eaton, J.K.: Experimental study of flow reattachment in a single-sided sudden expansion. Report MD-41, Department of Mechanical Engineering, Stanford University, 1984.

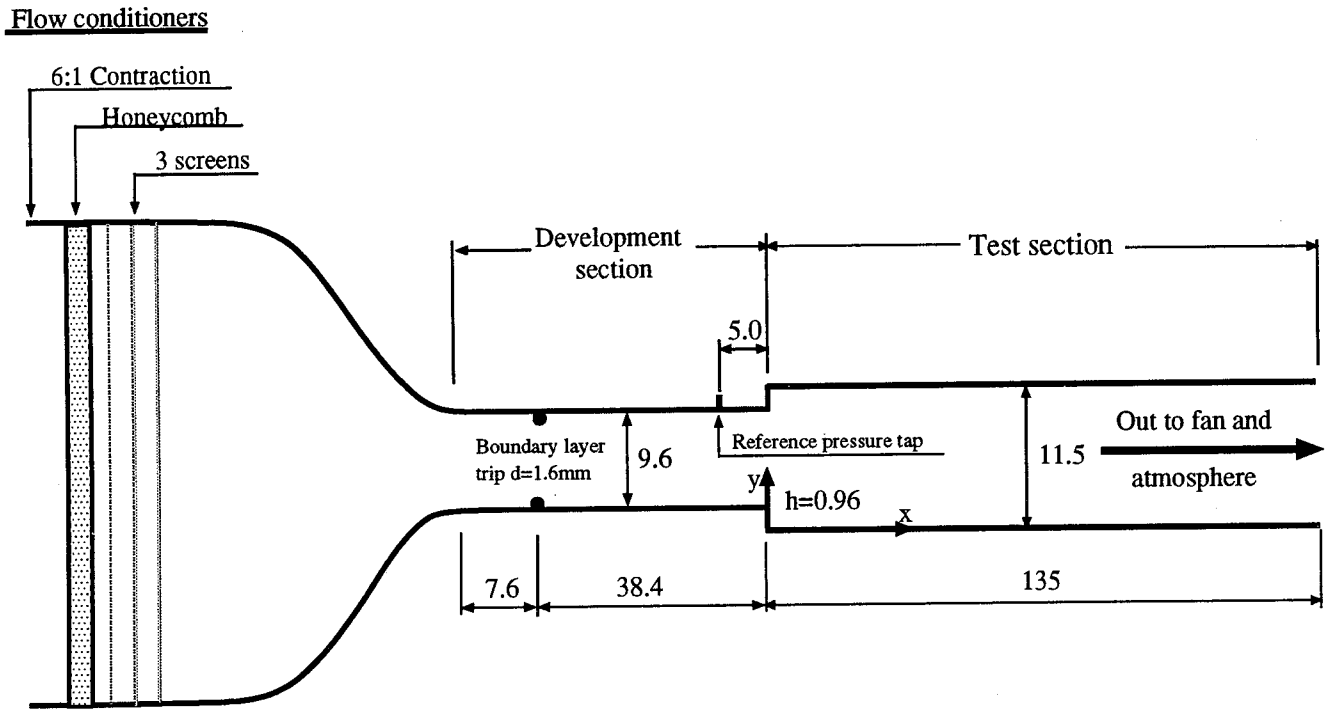

Figure 1. Wind tunnel schematic (all dimensions are in centimeters; drawing is not to scale).

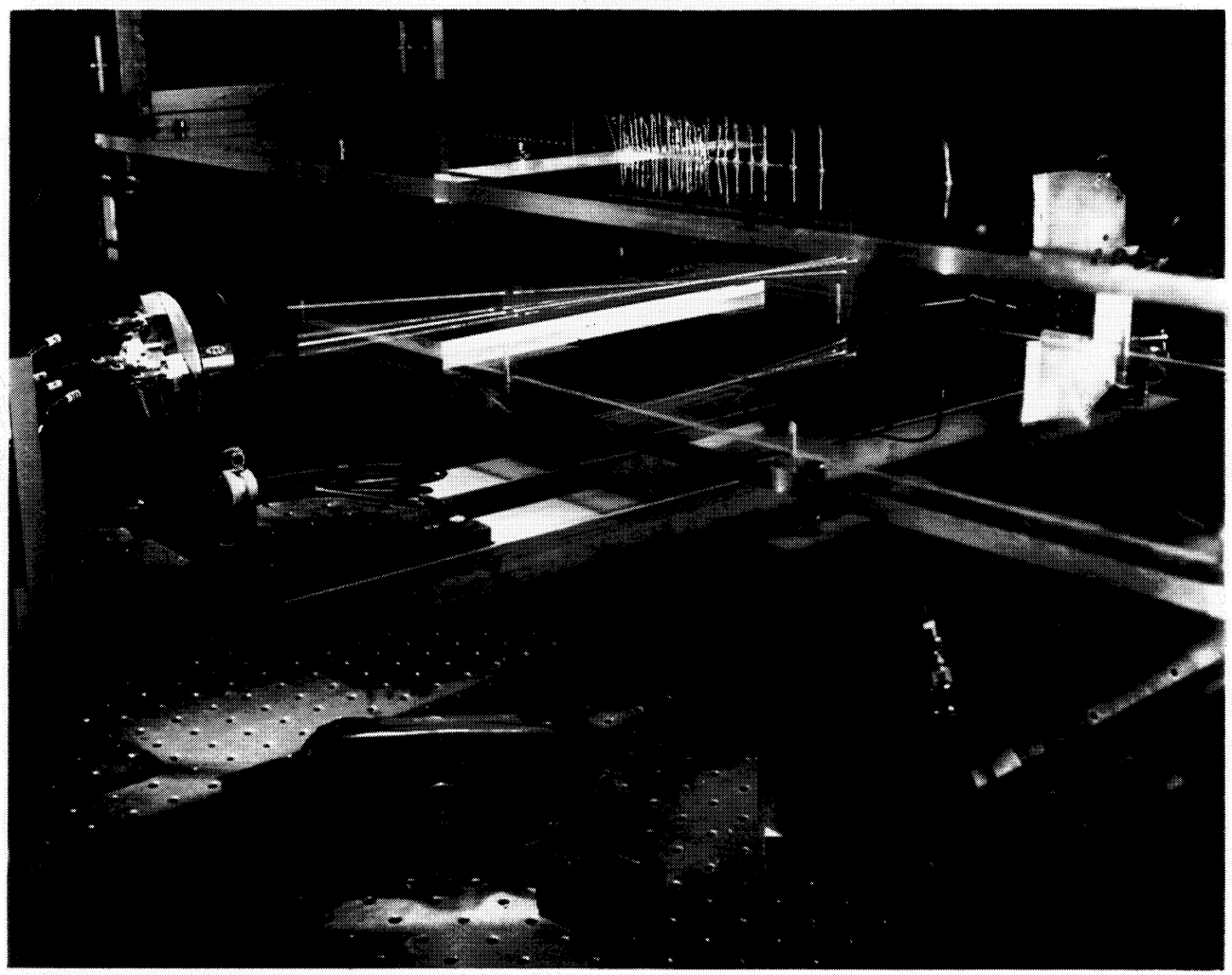

Figure 2. Photograph of the laser Doppler velocimeter.

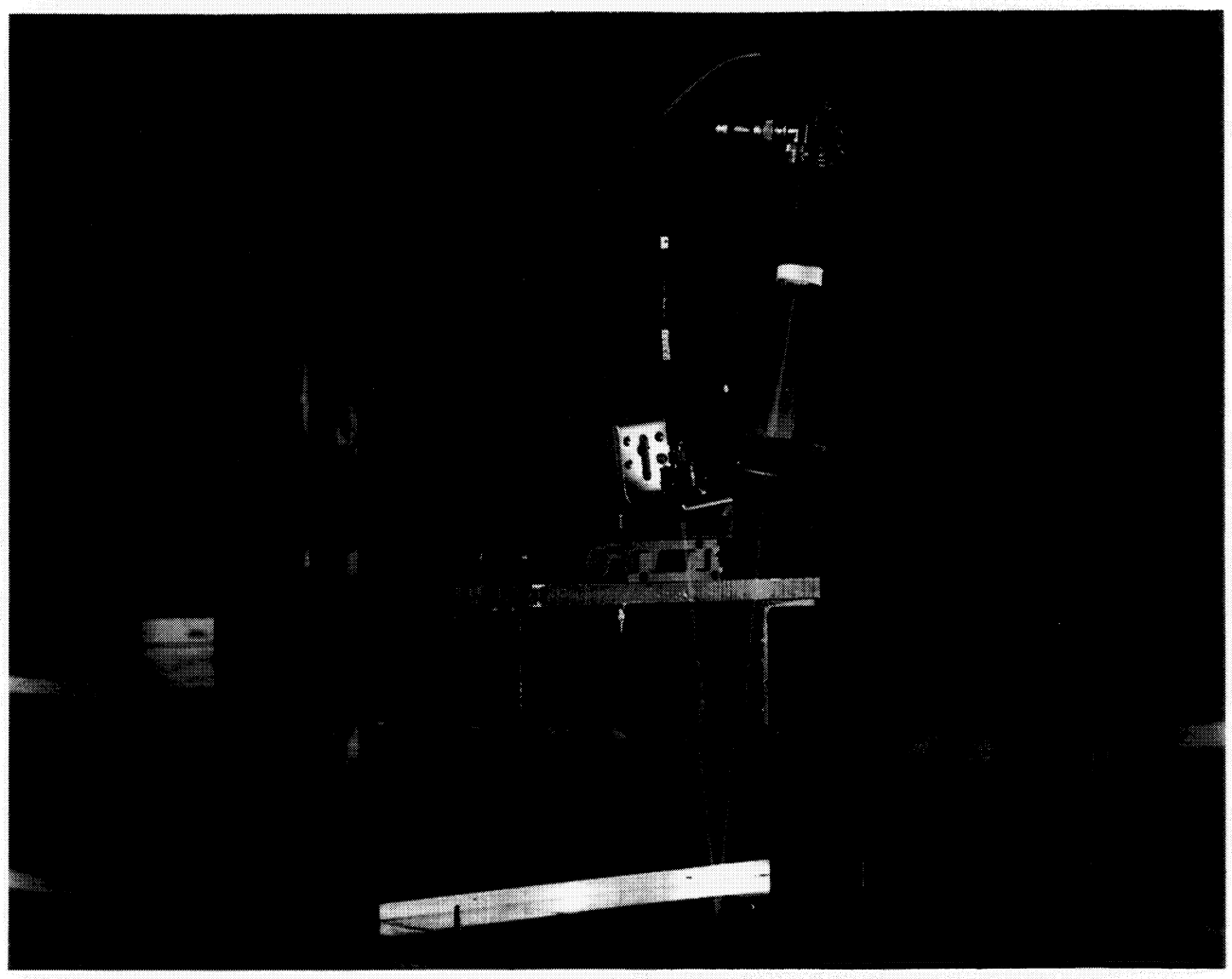

Figure 3. Photograph of oil-flow interferometer for measuring skin friction.

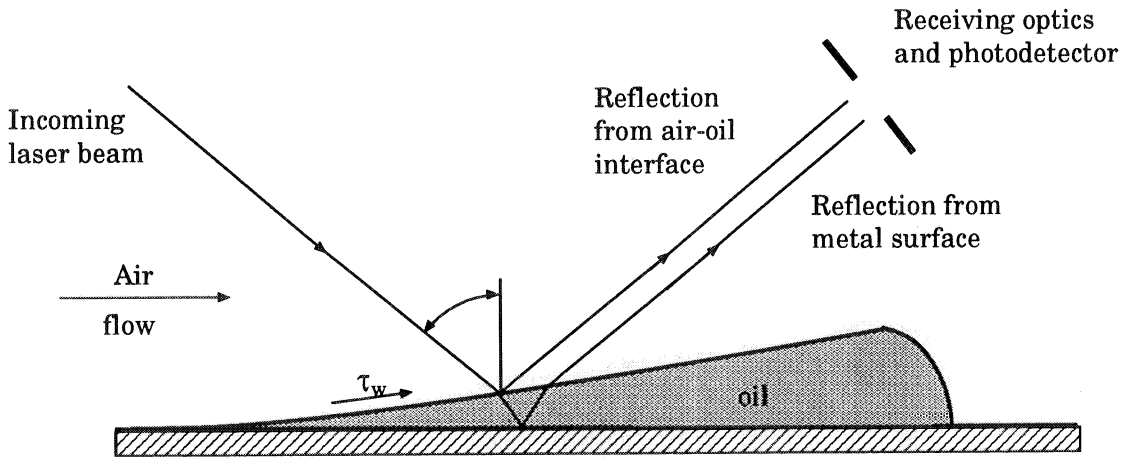

Figure 4. Laser oil-flow interferometer technique for measuring skin friction.

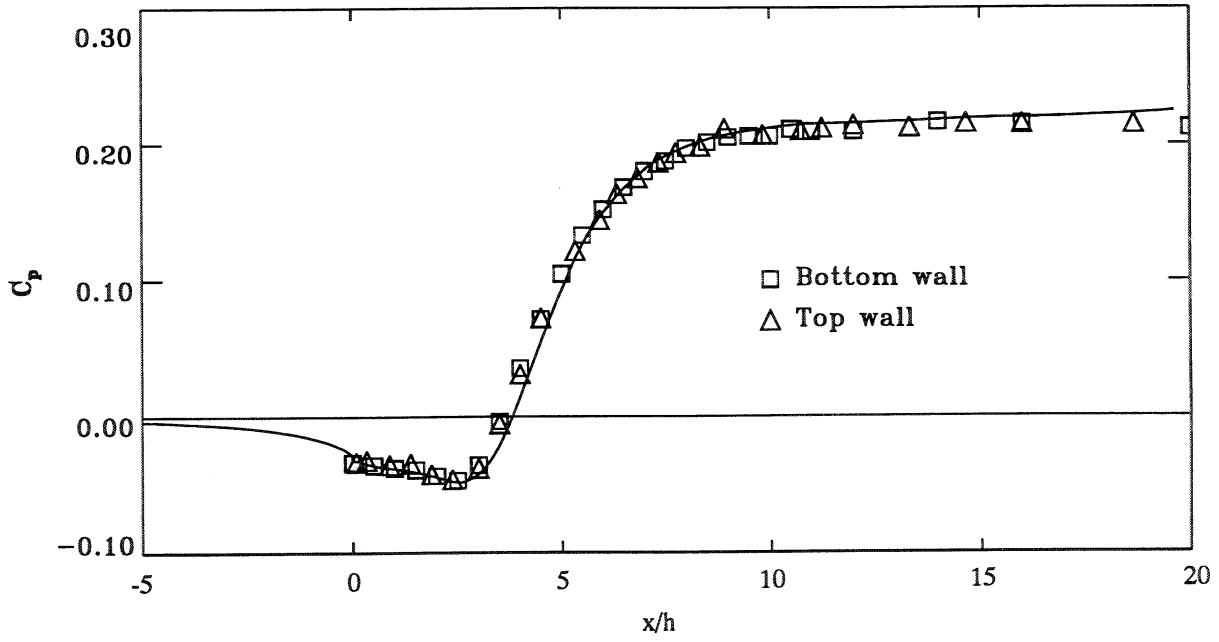

Figure 5. Distribution of pressure coefficient along top and bottom walls downstream of the step. Solid line represents pressure distribution obtained by the simulation.

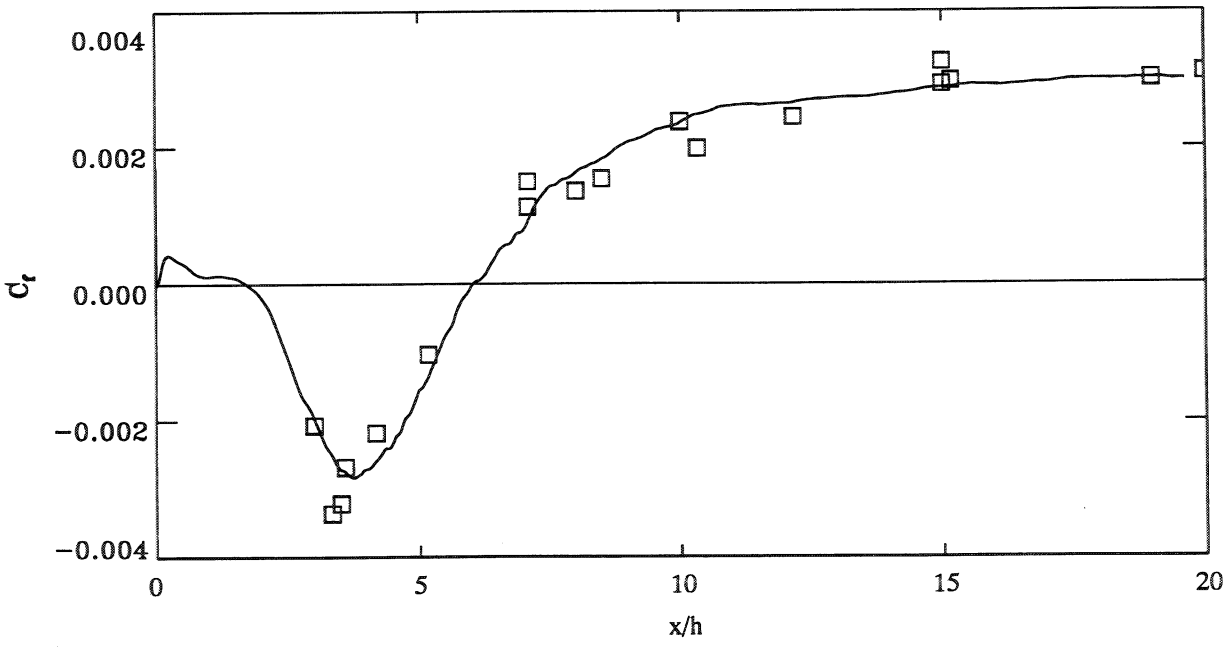

Figure 6. Distribution of skin–friction coefficient in the streamwise direction. Solid line represents skin–friction coefficient obtained by the simulation.

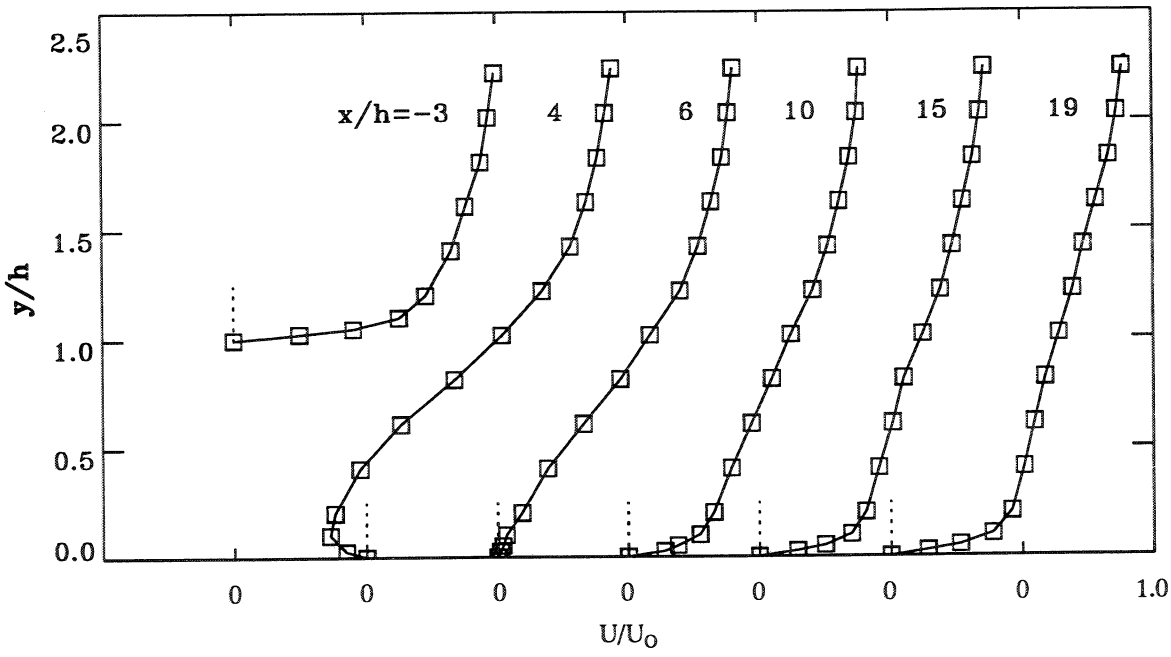

Figure 7. Profiles of mean streamwise velocity profiles for seven measuring stations. Solid lines are for visual aid only. Note the shift in the streamwise direction for each profile.

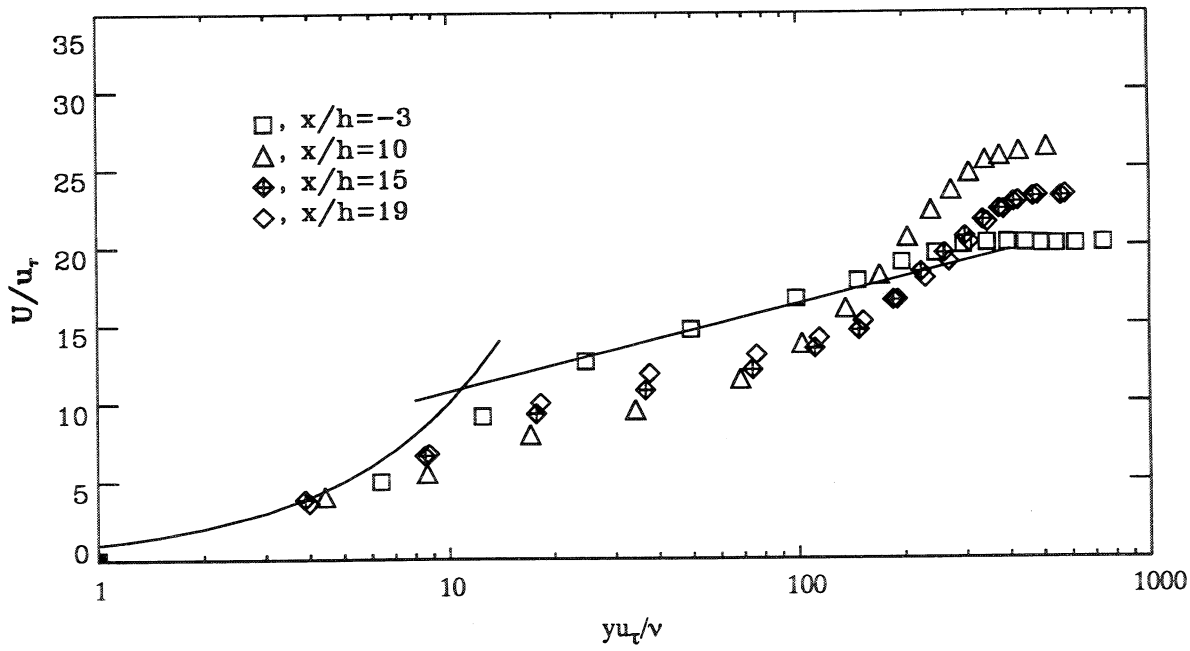

Figure 8. Mean velocity profiles in wall coordinates in the recovery region. Solid line represent standard liner and log relationships in the inner layer.

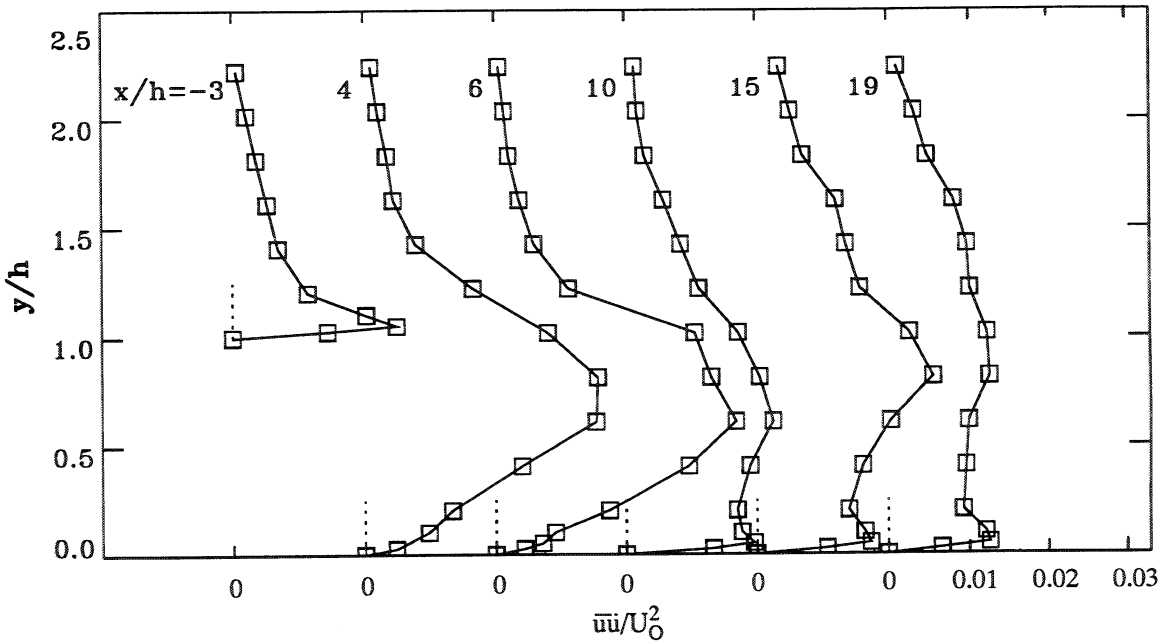

Figure 9. Profiles of $\overline{uu}/U^2_o$ at seven measuring stations. Solid lines are for visual aid only. Note the shift in the streamwise direction for each profile.

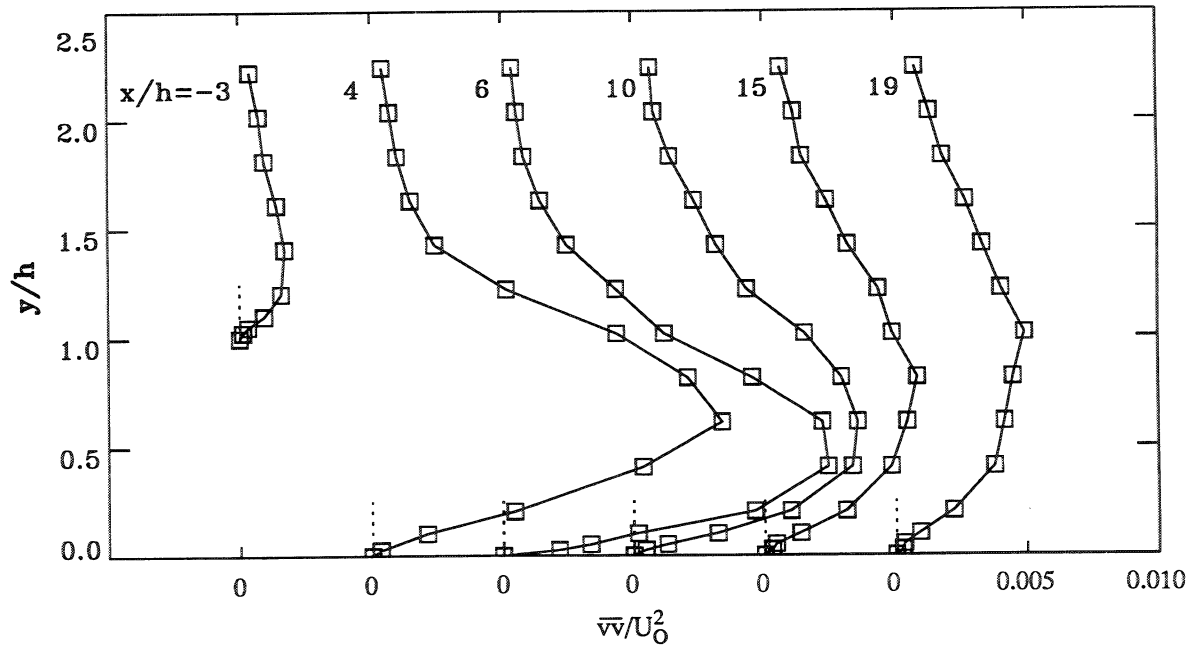

Figure 10. Profiles of $\overline{vv}/U^2_o$ at seven measuring stations. Solid lines are for visual aid only. Note the shift in the streamwise direction for each profile.

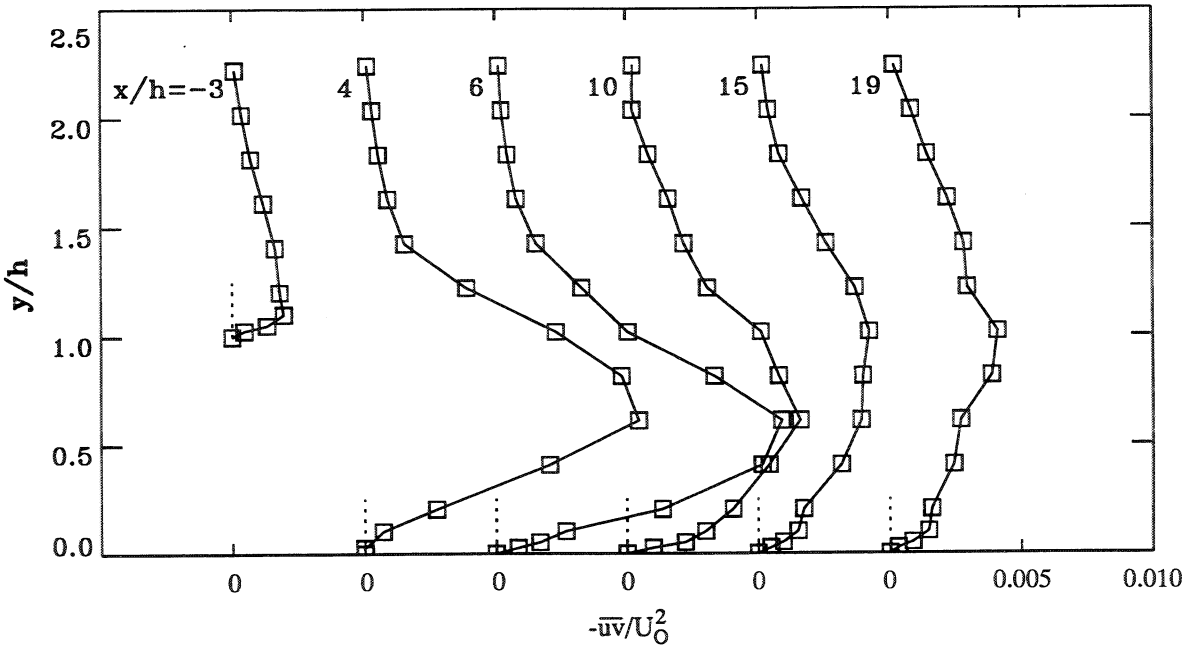

Figure 11. Profiles of $-\overline{uv}/U^2_o$ at seven measuring stations. Solid lines are for visual aid only. Note the shift in the streamwise direction for each profile.

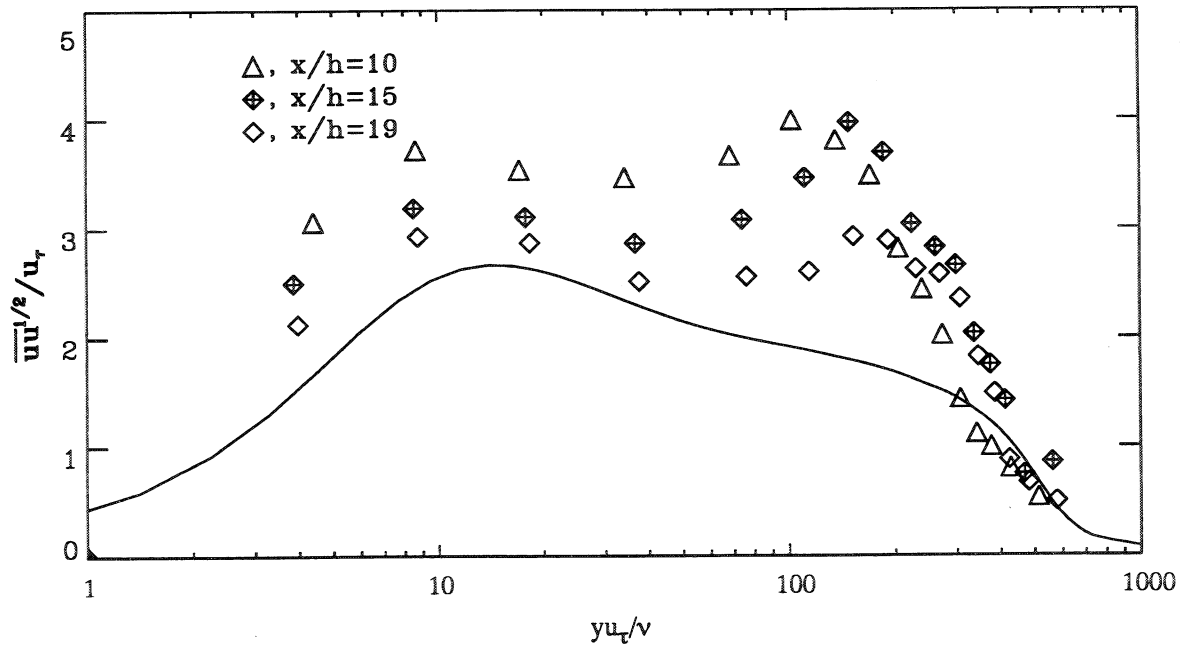

Figure 12. Normal stress $\overline{uu}$ profiles in wall coordinates in the recovery region. Solid line denotes simulation by Spalart for Re_θ=1410.

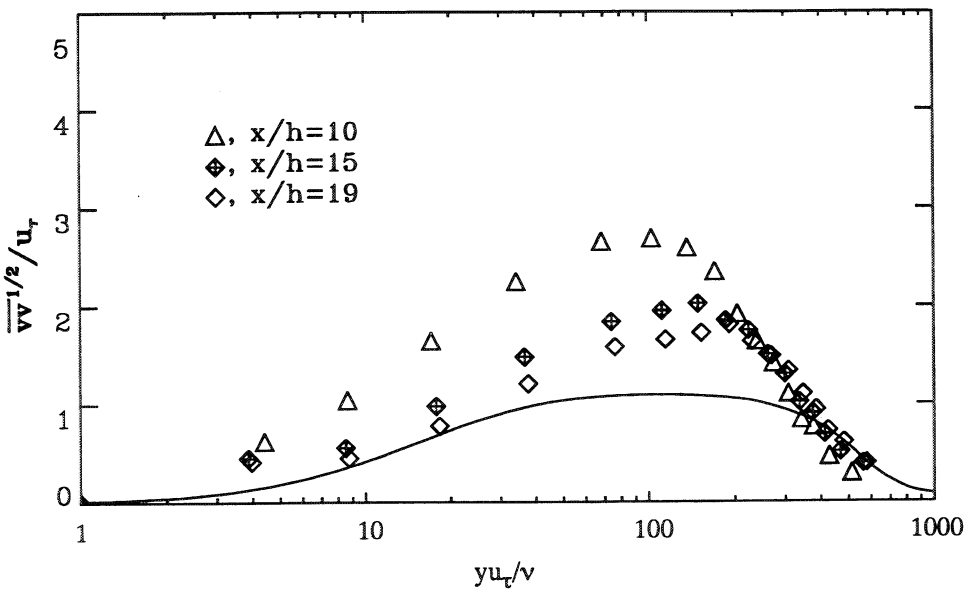

Figure 13. Normal stress $\overline{vv}$ profiles in wall coordinates in the recovery region. Solid line denotes simulation by Spalart for Re_θ=1410.

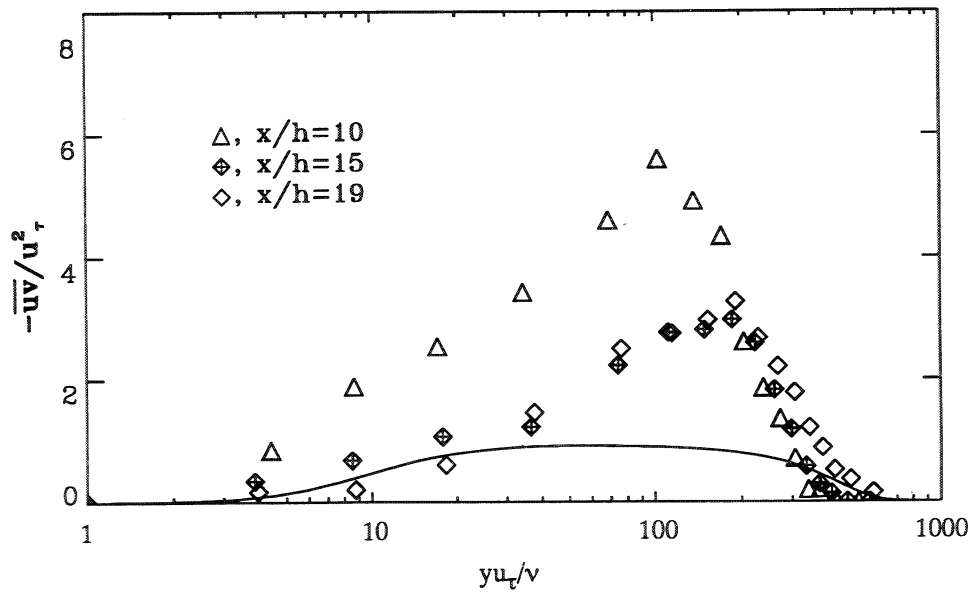

Figure 14. Shear stress profiles in wall coordinates in the recovery region. Solid line denotes simulation by Spalart for Re_θ=1410.

Appendix

U_0=7.72m/s h=0.98cm Re_h= 5000 x_r/h= 6.0

Reference wall static pressure is measured in x/h=-5.1
Reference velocity U_0 is measured in x/h=-3.05

Table 1: Integral parameters

x/h	U_e(m/s)	δ^*(mm)	θ(mm)	δ(mm)	H	Re_θ	10^3*C_f	G
-3.05	7.72	1.73	1.19	11.5	1.45	610	4.90	6.24
4.0	7.41	10.47	1.96	22.0	5.33	970	-2.72	N/A
6.0	7.12	8.41	2.98	21.0	2.82	1416	0.00	N/A
10.0	6.97	6.53	3.46	22.5	1.89	1608	2.35	13.71
15.0	6.75	5.95	3.52	24.0	1.69	1585	2.83	10.85
19.0	6.95	5.80	3.56	24.0	1.63	1651	3.00	9.97

Table 2: C_f measurements

x/h	C_f
3.0	-0.00207
3.33	-0.00336
3.50	-0.00321
3.58	-0.00268
4.17	-0.00218
5.17	-0.00103
7.08	0.00113
7.08	0.00150
8.00	0.00136
8.50	0.00154
10.0	0.00237

Table 2: C_f measurements

x/h	C_f
10.33	0.00198
12.17	0.00244
15.00	0.00292
15.00	0.00325
15.17	0.00297
19.00	0.0030
20.00	0.0031

Table 3: Pressure coefficient along the bottom wall of the tunnel

#pt	x/h	C_p
1	0.0	-0.0340
2	0.5	-0.0360
3	1.0	-0.0380
4	1.5	-0.0392
5	2.0	-0.0437
6	2.5	-0.0471
7	3.0	-0.0357
8	3.5	-0.0038
9	4.0	0.0357
10	4.5	0.0715
11	5.0	0.1046
12	5.5	0.1331
13	6.0	0.1521
14	6.5	0.1681
15	7.0	0.1798
16	7.5	0.1871
17	8.0	0.1966
18	8.5	0.2008
19	9.0	0.2046

Table 3: Pressure coefficient along the bottom wall of the tunnel

#pt	x/h	C_p
20	9.5	0.2053
21	10.0	0.2053
22	10.5	0.2103
23	11.0	0.2087
24	12.0	0.2091
25	14.0	0.2160
26	16.0	0.2148
27	20.0	0.2118
28	24.0	0.2148
29	28.0	0.2160
30	32.0	0.2160

Table 4: Pressurre coefficient along the top wall of the tunnel

#pt	x/h	C_p
1	0.083	-0.0335
2	0.333	-0.0323
3	0.875	-0.0354
4	1.375	-0.0346
5	1.875	-0.0426
6	2.375	-0.0464
7	3.000	-0.0380
8	3.500	-0.0057
9	4.000	0.0312
10	4.500	0.0722
11	5.333	0.1217
12	5.917	0.1445
13	6.333	0.1635
14	6.833	0.1749
15	7.333	0.1863
16	7.750	0.1932

Table 4: Pressurre coefficient along the top wall of the tunnel

#pt	x/h	C_p
17	8.333	0.1977
18	8.917	0.2110
19	9.833	0.2065
20	10.75	0.2095
21	11.25	0.2114
22	12.00	0.2137
23	13.33	0.2122
24	14.667	0.2152
25	16.00	0.2148
26	18.667	0.2148
27	21.333	0.2179
28	32.00	0.2186

Table 5: Measurements at x/h= -3.12

y (mm)	U (m/s)	V (m/s)	uu (m^2/s^2)	vv (m^2/s^2)	-uv (m^2/s^2)
0.25	1.91	0.00	0.711	0.008	0.027
0.49	3.49	0.00	1.232	0.019	0.078
0.97	4.83	-0.01	1.003	0.055	0.115
1.94	5.61	0.00	0.563	0.093	0.106
3.88	6.36	0.01	0.341	0.101	0.096
5.82	6.79	0.04	0.260	0.083	0.070
7.76	7.24	0.04	0.179	0.056	0.042
9.70	7.46	0.08	0.105	0.044	0.022
11.64	7.66	0.07	0.031	0.024	0.006
13.58	7.71	0.06	0.011	0.013	0.000
15.52	7.72	0.06	0.008	0.010	-0.001
17.46	7.71	0.04	0.007	0.010	-0.001
19.40	7.69	0.03	0.012	0.010	0.000
21.34	7.68	0.04	0.012	0.009	-0.001
24.25	7.68	0.06	0.006	0.008	0.000
29.10	7.71	0.02	0.006	0.009	0.000
28.80	7.70	-0.01	0.007	0.008	0.000

Table 6: Measurements at x/h= 4

y(mm)	U (m/s)	V (m/s)	uu (m^2/s^2)	vv (m^2/s^2)	-uv (m^2/s^2)
0.25	-0.59	0.02	0.236	0.019	-0.001
0.97	-1.06	-0.04	0.481	0.124	0.041
1.94	-0.92	-0.09	0.658	0.323	0.162
3.88	-0.18	-0.22	1.189	0.615	0.418
5.82	1.02	-0.43	1.755	0.794	0.620
7.76	2.60	-0.49	1.766	0.717	0.582
9.70	4.00	-0.51	1.389	0.556	0.433
11.64	5.19	-0.44	0.820	0.306	0.230
13.58	6.03	-0.39	0.387	0.144	0.091
15.52	6.50	-0.36	0.221	0.089	0.053
17.46	6.84	-0.32	0.171	0.059	0.032
19.40	7.07	-0.29	0.102	0.042	0.018
21.34	7.27	-0.25	0.053	0.026	0.007
24.25	7.38	-0.21	0.017	0.014	0.001
29.10	7.36	-0.16	0.011	0.011	0.000
28.80	7.41	-0.09	0.009	0.007	0.001

Table 7: Measurements at x/h= 6

y (mm)	U (m/s)	V (m/s)	uu (m^2/s^2)	vv (m^2/s^2)	-uv (m^2/s^2)
0.25	0.08	-0.08	0.218	0.127	0.050
0.49	0.16	-0.08	0.356	0.199	0.099
0.97	0.26	-0.12	0.452	0.306	0.158
1.94	0.72	-0.20	0.862	0.572	0.377
3.88	1.49	-0.33	1.464	0.737	0.603
5.82	2.55	-0.47	1.823	0.724	0.647
7.76	3.64	-0.53	1.635	0.566	0.495
9.70	4.51	-0.45	1.511	0.367	0.299
11.64	5.40	-0.39	0.556	0.258	0.195
13.58	5.94	-0.37	0.296	0.147	0.092
15.52	6.33	-0.34	0.185	0.087	0.047
17.46	6.65	-0.31	0.105	0.050	0.027

Table 7: Measurements at x/h= 6

y (mm)	U (m/s)	V (m/s)	uu (m^2/s^2)	vv (m^2/s^2)	-uv (m^2/s^2)
19.40	6.83	-0.28	0.070	0.034	0.014
21.34	6.98	-0.26	0.031	0.024	0.008
24.25	7.07	-0.23	0.012	0.010	0.001
29.10	7.11	-0.19	0.009	0.005	0.001
38.80	7.17	-0.15	0.009	0.005	0.001

Table 8: Measurements at x/h= 10

y (mm)	U (m/s)	V (m/s)	uu (m^2/s^2)	vv (m^2/s^2)	-uv (m^2/s^2)
0.25	1.07	-0.01	0.658	0.027	0.059
0.49	1.46	-0.04	0.968	0.076	0.132
0.97	2.11	-0.08	0.875	0.190	0.178
1.94	2.52	-0.13	0.840	0.356	0.240
3.88	3.04	-0.21	0.939	0.495	0.322
5.82	3.64	-0.26	1.114	0.507	0.392
7.76	4.24	-0.30	1.013	0.471	0.344
9.70	4.80	-0.21	0.850	0.388	0.304
11.64	5.44	-0.21	0.555	0.258	0.183
13.58	5.89	-0.12	0.418	0.189	0.130
15.52	6.23	-0.09	0.287	0.140	0.095
17.46	6.53	-0.06	0.145	0.085	0.050
19.40	6.74	-0.06	0.088	0.049	0.014
21.34	6.81	-0.07	0.070	0.041	0.015
24.25	6.89	-0.06	0.045	0.015	0.002
29.10	6.96	-0.10	0.020	0.006	0.000
38.80	6.99	-0.08	0.026	0.005	0.000

Table 9: Measurements at x/h= 15

y (mm)	U (m/s)	V (m/s)	uu (m^2/s^2)	vv (m^2/s^2)	-uv (m^2/s^2)
0.25	1.12	0.00	0.528	0.017	0.029
0.49	1.93	0.00	0.857	0.026	0.057
0.97	2.70	-0.01	0.813	0.081	0.090
1.94	3.13	-0.04	0.693	0.185	0.103
3.88	3.51	-0.07	0.800	0.286	0.188
5.82	3.91	-0.13	1.009	0.322	0.233
7.76	4.24	-0.11	1.328	0.345	0.237
9.70	4.80	-0.13	1.149	0.289	0.251
11.64	5.32	-0.12	0.779	0.258	0.219
13.58	5.67	-0.09	0.674	0.190	0.154
15.52	5.98	-0.05	0.597	0.142	0.100
17.46	6.28	-0.01	0.350	0.087	0.049
19.40	6.48	0.03	0.258	0.069	0.025
21.34	6.61	0.05	0.171	0.040	0.012
24.25	6.71	0.06	0.047	0.022	0.001
29.10	6.72	0.06	0.062	0.013	0.001
38.80	6.77	0.04	0.085	0.009	0.002

Table 10: Measurements at x/h= 19

y (mm)	U (m/s)	V (m/s)	uu (m^2/s^2)	vv (m^2/s^2)	-uv (m^2/s^2)
0.25	1.08	0.01	0.403	0.015	0.019
0.49	2.02	0.00	0.765	0.018	0.051
0.97	2.98	0.00	0.735	0.054	0.087
1.94	3.54	-0.01	0.565	0.130	0.094
3.88	3.90	-0.01	0.585	0.223	0.144
5.82	4.21	-0.02	0.606	0.245	0.160
7.76	4.53	-0.06	0.763	0.265	0.230
9.70	4.94	-0.07	0.745	0.292	0.243
11.64	5.35	-0.05	0.616	0.239	0.175
13.58	5.66	-0.03	0.595	0.197	0.167
15.52	6.03	-0.02	0.495	0.159	0.130

Table 10: Measurements at x/h= 19

y (mm)	U (m/s)	V (m/s)	uu (m^2/s^2)	vv (m^2/s^2)	-uv (m^2/s^2)
17.46	6.41	0.02	0.297	0.108	0.084
19.40	6.65	0.02	0.198	0.079	0.049
21.34	6.82	0.06	0.069	0.047	0.011
24.25	6.92	0.09	0.040	0.033	0.006
29.10	6.94	0.11	0.022	0.014	0.001
38.80	6.97	0.09	0.015	0.008	0.000

REPORT DOCUMENTATION PAGE

Form Approved
OMB No. 0704-0188

1. AGENCY USE ONLY *(Leave blank)*	2. REPORT DATE	3. REPORT TYPE AND DATES COVERED
	February 1994	Technical Memorandum

4. TITLE AND SUBTITLE

Backward-Facing Step Measurements at Low Reynolds Number, Re_h=5000

5. FUNDING NUMBERS

505-59-50

6. AUTHOR(S)

Srba Jovich and David M. Driver

7. PERFORMING ORGANIZATION NAME(S) AND ADDRESS(ES)

Ames Research Center
Moffett Field, CA 94035-1000

8. PERFORMING ORGANIZATION REPORT NUMBER

A-94043

9. SPONSORING/MONITORING AGENCY NAME(S) AND ADDRESS(ES)

National Aeronautics and Space Administration
Washington, DC 20546-0001

10. SPONSORING/MONITORING AGENCY REPORT NUMBER

NASA TM-108807

11. SUPPLEMENTARY NOTES

Point of Contact: Srba Jovich, Ames Research Center, MS 229-1, Moffett Field, CA 94035-1000; (415) 604-6192

12a. DISTRIBUTION/AVAILABILITY STATEMENT

Unclassified — Unlimited
Subject Category 34

12b. DISTRIBUTION CODE

13. ABSTRACT ***(Maximum 200 words)***

An experimental study of the flow over a backward-facing step at low Reynolds number was performed for the purpose of validating a direct numerical simulation (DNS) which was performed by the Stanford/NASA Center for Turbulence Research. Previous experimental data on backstep flows were conducted at Reynolds numbers and/or expansion ratios which were significantly different from that of the DNS.

The geometry of the experiment and the simulation were duplicated precisely, in an effort to perform a rigorous validation of the DNS. The Reynolds number used in the DNS was Re_h=5100 based on step height, h. This was the maximum possible Reynolds number that could be economically simulated. The boundary layer thickness, d,was approximately 1.0h in the simulation and the expansion ratio was 1.2. The Reynolds number based on the momentum thickness, Re_θ, upstream of the step was 610. All of these parameters were matched experimentally.

Experimental results are presented in the form of tables, graphs and a floppy disk (for easy access to the data). An LDV instrument was used to measure mean velocity components and three Reynolds stresses components. In addition, surface pressure and skin friction coefficients were measured. LDV measurements were acquired in a measuring domain which included the recirculating flow region.

14. SUBJECT TERMS

LDV measurements (Laser DopplerVelocimeter), Separated Flows, Backward-Facing Step, DNS Code Validation (Direct Numerical Simulation)

15. NUMBER OF PAGES

28

16. PRICE CODE

A03

17. SECURITY CLASSIFICATION OF REPORT	18. SECURITY CLASSIFICATION OF THIS PAGE	19. SECURITY CLASSIFICATION OF ABSTRACT	20. LIMITATION OF ABSTRACT
Unclassified	Unclassified		